Development of a Transportable Telescope for Galactic Survey at 500 GHz in Antarctica

Shun Ishii, Masumichi Seta, Naomasa Nakai, Yusuke Miyamoto, Makoto Nagai, Hitoshi Arai, Hiroyuki Maezawa, Taketo Nagasaki, Naoki Miyagawa, Hideaki Motoyama, Yutaro Sekimoto, and Leonardo Bronfman

***Abstract*—We have developed a transportable 30-cm submillimeter-wave telescope to operate at the Dome Fuji station in the Antarctic plateau. Transportability is an important requirement in the design; the telescope can be divided into several subsystems by hands. The maximum weight of the subsystems is restricted to be below 60 kg, so that the telescope can be assembled without a lifting machine. A small 4 K mechanical cryocooler is used for cooling down a SIS mixer. Total power consumption was designed to be less than 2.5 kW. The optical system was designed to satisfy the frequency independent matching condition at the subreflector and the feed horn of the SIS mixer, so we could accommodate a higher frequency receiver without changing mirrors. A quasi-optical filter was employed for the single sideband operation in observations of the CO $(J = 4-3)$ line at 461.04 GHz and the [CI] $(^3P_1-^3P_0)$ line at 492.16 GHz. It was equipped with a 1 GHz width spectrometer that covers a velocity width of 600 km/s with a velocity resolution of 0.04 km/s at 461 GHz. We carried out test observations at a 4400-m altitude site in northern Chile during winters of 2010 and 2011. The typical system noise temperature, including atmospheric loss, was 3000 K (SSB) at 461 GHz, that is mainly limited by atmospheric opacity. The beam size of the 30-cm offset Cassegrain antenna at 0.65 mm of wavelength was measured to be $9'.4 \pm 0'.4$ by cross scanning of the sun. This angular resolution of the 30-cm telescope is same as those of the Columbia-CfA-U. Chile CO $(J = 1-0)$ surveys. We estimated the main beam efficiency to be $87 \pm 5\%$ by observing the new moon. We succeeded in mapping Orion Molecular Cloud A and M17 SW in CO $(J = 4-3)$ followed by test observations toward Orion KL in both CO $(J = 4-3)$ and [CI] $(^3P_1-^3P_0)$.**

***Index Terms*—Astronomy, astrophysics, submillimeter-wave technology .**

Manuscript received July 01, 2012; revised November 29, 2012; accepted December 11, 2012. Date of publication January 23, 2013; date of current version February 07, 2013. This work was supported in part by Grant-in-Aid for Scientific research A from JSPS under 19204016 and Toray Science and Technology under Grant (06-4704). The work of S. Ishii was supported by JSPS for Young Scientists. The work of L. Bronfman was supported by CONICYT Project PFB06.

S. Ishii, M. Seta, N. Nakai, Y. Miyamoto, M. Nagai, H. Arai, T. Nagasaki, and N. Miyagawa are with Institute of Physics, University of Tsukuba, Tsukuba, Ibaraki 305-8571, Japan (e-mail: ishii.shun.fw@u.tsukuba.ac.jp).

H. Maezawa is with the Physical Science, Osaka Prefecture University, Gakuen-cho, Naka-ku, Sakai-shi, Osaka 599-8531, Japan.

H. Motoyama is with National Institute of Polar Research, 10-3 Midoricho, Tachikawa, Tokyo 190-8518, Japan.

Y. Sekimoto is with National Astronomical Observatory of Japan, Mitaka, Tokyo 181-8588, Japan.

L. Bronfman is with Departamento de Astronomía, Universidad de Chile, Santiago Casilla 36-D, Chile.

Color versions of one or more of the figures in this paper are available online at http://ieeexplore.ieee.org.

Digital Object Identifier 10.1109/TTHZ.2012.2235912

I. Introduction

THE Galctic surveys are a fundamental approach to understand characteristics of interstellar medium in the Milky Way. In the millimeter-wave region, several surveys have revealed its mass, distribution, kinematic information and the physical properties. The Colombia-CfA-U. Chile 1.2 m telescopes identified giant molecular clouds (GMCs) throughout the Milky Way in the CO $(J = 1-0)$ line at 115 GHz [1]–[3]. The Massachusetts-Stony Brook Galactic CO surveys essentially detected all clouds of size larger than 20 pc in $8° < l < 90°$ [4]. A 60 cm telescope named AMANOGAWA telescope surveyed in the CO $(J = 2-1)$ line at 230 GHz [5], [6]. Physical parameters of GMCs such as temperature and density are derived by intensity ratio of molecular lines in different transitions. They found a global decrease of gas density with increasing the distance from the Galactic center.

Submillimeter CO lines (e.g., 345, 461, and 691 GHz) are preferable to restrict physical condition of GMCs. Atomic carbon and nitrogen may be good probes for the atomic phase of interstellar medium. Although some telescopes observed the Milky Way, the observed area is limited only around the Galactic center [7], on the Galactic equator [8] and on some major GMCs because the atmosphere is very opaque for submillimeter waves.

A dryer and higher altitude site is needed for submillimeter-wave observations. The atmospheric transparency is mainly determined by the amount of water vapor and oxygen. Several sites with better atmospheric transparency have been developed such as Mauna Kea in Hawaii, USA, and the Andes plateau close to the Atacama Desert in Chile. The atmospheric transparency at these sites is not high and stable enough for continuous submillimeter-wave observations above 450 GHz. The Antarctic plateau is a good site for a Galactic plane survey in submillimeter wave. We have developed a transportable telescope for this new survey in the CO $(J = 4-3)$ line at 461.04 GHz and the [CI]$(^3P_1-^3P_0)$ line at 492.16 GHz in 500 GHz band. In this paper we describe the design of the telescope for operation in Antarctica and show results of the performance in test observations.

II. Dome Fuji Station in the Antarctic Plateau

Japanese Antarctic station, the Dome Fuji station, is expected to be one of the best sites for submillimeter-wave astronomy because of its high altitude of 3800 m and low average temperature of -54 °C [9]. Dome Fuji is located in latitude 77° 19' S and longitude 39° 42' E [10]. Dome Fuji was established in 1995 by Japanese Antarctic Research Expedition for drilling ice cores to

2156-342X/$31.00 © 2013 IEEE

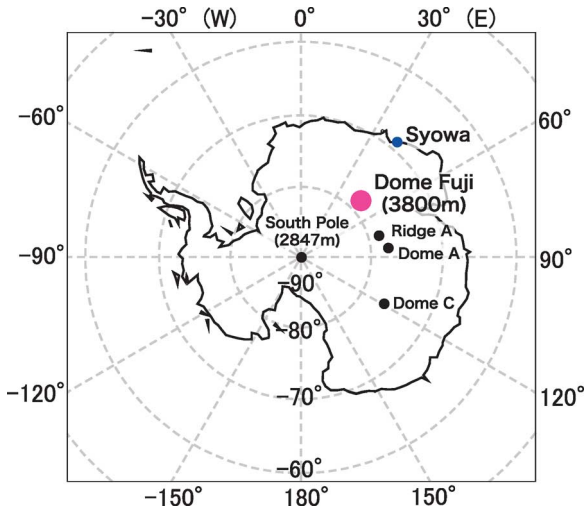

Fig. 1. Location of Dome Fuji and other sites in Antarctica.

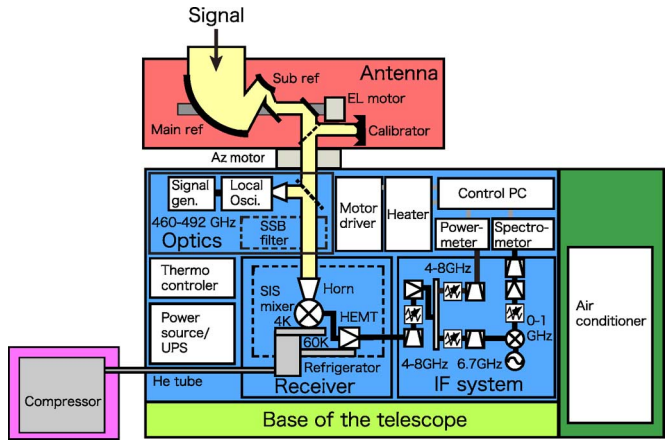

Fig. 2. Block diagram of the system of the 30-cm telescope. The individual subsystem is shown with different colors.

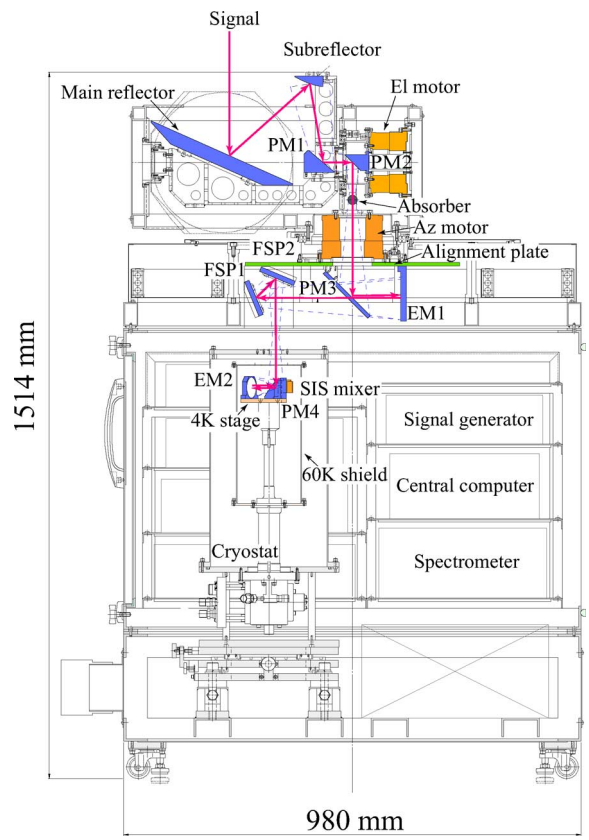

Fig. 3. Schematic drawing of the system of the 30-cm telescope. Blue-dashed line between mirrors represents the size of the beam at the edge taper of −40 dB.

study a long-term variation of climate. It is about 1000 km away from a Japanese station at the coast, Syowa. Basic transportation means are snow vehicles and sledges, although Dome Fuji is accessible by a small plane. Currently, a telescope must be assembled without a lifting machine at Dome Fuji. The capacity of electric power is limited. Fig. 1 shows the location of Dome Fuji and other stations on a map of Antarctica where astronomical observation could be conducted. Although several test observations have been carried out at these stations, radio observations have been done only at the South Pole. The 1.7 m AST/RO telescope mapped the Galactic center in submillimeter lines [7]. The 10 m South Pole Telescope is operated to investigate the CMB anisotropy using millimeter/submillimeter-waves.

It has been known that the average fraction of the sky obscured by clouds was 30% in 1995–1997 [9]. The mean wind speed is 5.8 m/s [9] and hardly exceeds 10 m/s. The zenith opacity at 220 GHz in summer was very low and stable ($\tau_{220} = 0.045 \pm 0.007$), much better than that of Atacama plateau in Chile in their same seasons, and is comparable in their best seasons [11]. We showed in simulations that several submillimeter atmospheric windows between 340 and 1000 GHz open through a whole year. Several THz windows open in winter at 1.0–2.0 THz. Furthermore, low fluctuation of the opacity is an advantage of Dome Fuji. This enables us to continue a submillimeter-wave observation for a long time under good atmospheric conditions. Similar good transmission in submillimeter-wave length is obtained in Dome A [12]. For these advantages of the Antarctic plateau in topographic and climatic conditions, we are developing Dome Fuji as a site for astronomical observation from submillimeter to near-infrared region [13], [14].

III. The 30-cm Telescope

A. Configuration

The size for a main reflector of 30 cm is chosen to produce a 9′ beam at 461 GHz so that we can compare the data of the low-J CO surveys directly. Transportability is an important requirement to the 30-cm telescope for the operation at Dome Fuji. We designed the 30-cm telescope to be divided into several subsystems by hands. The maximum weight of each subsystem is restricted to be below 60 kg for fulfilling this requirement. We also set the upper limit on the total power consumption of 2.5 kW to satisfy the condition of the electric capacity at Dome Fuji. Fig. 2 shows a system diagram of the 30-cm telescope. We adopted a standard-type heterodyne radio telescope that consists of an antenna system, a local oscillator (LO), a mixer on a cryo-receiver, an intermediate frequency (IF) system, a back end system, and a control system.

Fig. 3 shows a schematic drawing of the configuration of systems in the 30-cm telescope. The antenna optical system

is placed on a box shaped main structure where the receiver system is accommodated. The beam from the antenna system (the main reflector and the subreflector) is reflected on the first plane mirror (PM1) and guided into the telescope along the elevation axis. The second plane mirror (PM2) reflects the beam to an alignment plate through a hollow of an azimuth motor. The plate holds the third plane mirror (PM3) and the first ellipsoidal mirror (EM1), a quasi-optical single sideband (SSB) filter, and a local oscillator system. It is mounted on an alignment reference plane under the antenna system directly to minimize misalignments.

A plane mirror (PM4) is placed on the 4 K stage of the receiver followed by an ellipsoidal mirror (EM2) and a feed horn. The position and tilt of the receiver are adjusted so as to achieve good alignment between the alignment plate on the antenna and the 4 K stage. The box also accommodates the IF system, the back end system, and the control system.

B. Optical System

1) Antenna System: The main reflector and a subreflector construct an offset Cassegrain antenna system. There is no blockage by the subreflector and its mount. This provides us with high main beam efficiency, that is important for the observation of broad and weak emission lines seen in the Galactic plane. The focal length of the main reflector is 258.40 mm. The subreflector is an offset hyperboloid with the eccentricity of 1.375 and its focal length of 166.39 mm. The diameter of the subreflector is 60.40 mm. We stipulated an edge taper level on the subreflector to be -17.0 dB, to suppress the side lobe level. We designed the antenna to implement the Mizuguchi condition for minimizing the cross-polarization loss and the Rusch condition for minimizing the spillover loss [15]. As a result, the axis of the subreflector tilts 1.311° respect to that of the main reflector. The synthetic focal length of the antenna system is 1627.91 mm. The effective focal ratio is 6.30 at the synthetic focus. All of mirrors are made of Al 5052 for ease of manufacture by the machining and the low-deformation characteristic. The surface accuracy of the main reflector and the subreflector is less than 5 μm. This accuracy enables us to observe a wavelength of $\sim$100 μm in the future.

Two direct-drive hollow motors were employed for driving the azimuth (Az) and the elevation (El) axis. The diameter of the hollow is 50 mm. The relative and absolute accuracy of positioning are $\pm 0.5''$ and $\pm 10''$, respectively. It is high accuracy enough to operate with angular resolution of $9'$. The low temperature under -20 °C would provoke damage to electronics of motors and grease in a bearing. We attached rubber heaters around motors and the bearing in order to solve this problem.

2) Transmission Optical System: We designed the transmission optical system that consists of elements from the subreflector to the feed horn, based on Gaussian beam propagation [16]. We also adopted a condition of frequency-independent matching between the subreflector and the feed horn [17]. The frequency-independent matching is a technique so that the beam parameters do not have frequency dependence at the surface of the subreflector and the aperture of the feed horn. In this technique a real image of the subreflector is formed on the aperture of the feed horn by ellipsoidal mirrors. This enables us to replace the receiver for an observation of higher frequency wave without a replacement of the optical system. We set the edge taper of mirrors after subreflector to -40.0 dB. The edge clearance of the beam to space in the telescope is set to -50.0 dB. We show the parameters of the optical system at 461.04 GHz in Table I and the calculated radius of the beam at 461 and 809 GHz in Fig. 4.

TABLE I
BEAM PARAMETERS OF OPTICAL SYSTEM AT 461.04 GHz

Element	z[a] (mm)	$w(z)$[b] (mm)	D(z)[c] (mm)	$R(z)$[d] (mm)
Main reflector	-252.75	–	300.00	–
Subreflector	0.00	19.73	60.40	306.80
Plane mirror 1 (PM1)	171.58	8.88	38.11	145.97
Plane mirror 2 (PM2)	234.38	5.27	22.61	101.40
Plane mirror 3 (PM3)	524.38	15.03	64.52	236.10
Elipsoidal mirror1 (EM1)	627.82	21.83	93.70	338.73 458.54
FSP1	901.38	9.29	37.87	207.63
FSP2	955.12	7.08	30.37	329.64
Window of the cryostat	1104.38	4.56	19.55	267.21
Plane mirror 4 (PM4)	1185.38	6.99	29.99	181.73
Elipsoidal mirror 2 (EM2)	1259.38	10.07	43.24	229.05 64.66
Feed horn	1318.38	1.50	–	20.00

[a] Distance from the position of the subreflector. The positive direction is taken to the feed horn.
[b] Beam radius.
[c] Diameter of a mirror (-40 / -17 dB) or clearance for space (-50 dB).
[d] Radius of curvature.

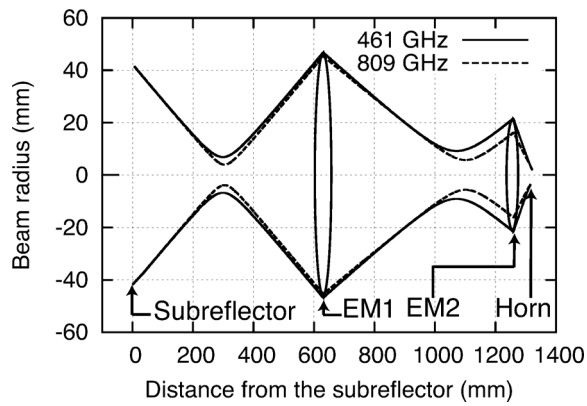

Fig. 4. Beam radius at an edge level of -40 dB.

We show a simulated beam pattern at 461.04 GHz in Fig. 5. The simulation was done with GRASP8 software packages using physical optics and physical theory of diffraction [18]. It calculates radiation from a mirror produced by the surface induced current on the mirror. We obtained the beam pattern of the telescope from calculations of the surface current and the radiation for all mirrors starting from ideal Gaussian beam pattern of the feed horn. The beam pattern has a symmetrical shape and a correct directionality. Its angular resolution (HPBW) is $9'.6$, which is comparable to the resolution of the Columbia-CfA-U. Chile telescopes and AMANOGAWA telescope. The level of a first side lobe is less than -32.0 dB, which is sufficiently low for the observation. The cross-polarization level is also low, less than -26.8 dB to the peak gain of the main-polarization pattern.

3) Feed Horn: We adopted a diagonal horn as the feed horn because it produces a good beam despite of easy manufacturing. Its coupling efficiency of the aperture field to the fundamental Gaussian mode is expected to be 84% and the side lobe level

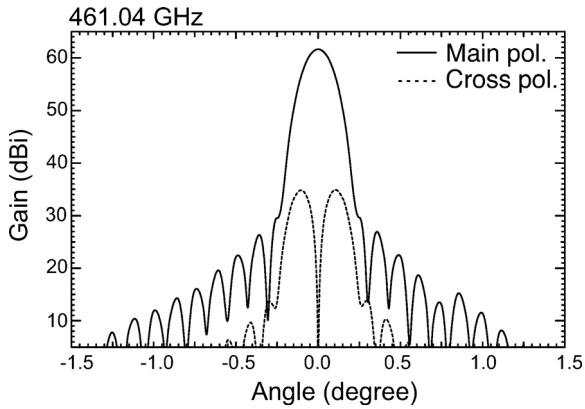

Fig. 5. Simulated beam pattern of the 30-cm telescope at 461.04 GHz.

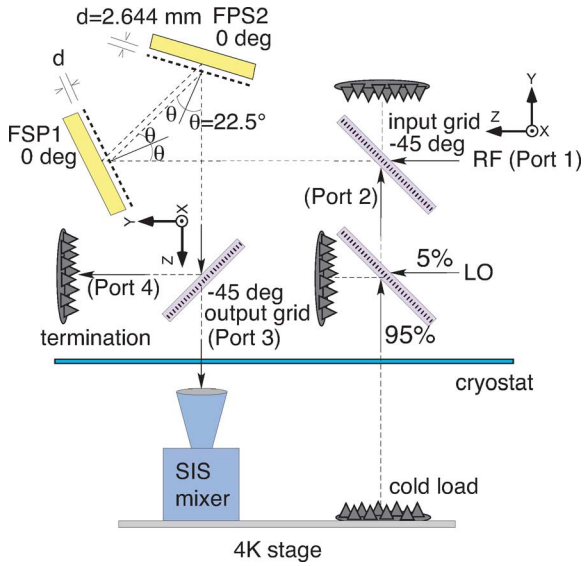

Fig. 6. Schematic view of the quasioptical SSB filter using FSPs.

is less than -25 dB [16]. We designed the horn to fit the beam parameters of the optical system based on Johansson and Whyborn [19]. The optimized aperture radius a and the slant length L of the horn are given by

$$\frac{w_h}{a} = 0.4316 \tag{1}$$

$$L = R_h \tag{2}$$

where w_h and R_h are the beam radius and the curvature of Gaussian beam at the aperture of the horn. Using these relations, we obtained the aperture radius as $a = 3.48$ mm and the slant length as $L = 20.00$ mm.

4) SSB Filter and LO Injection: The observation is done with the SSB mode to measure the intensity of lines in high accuracy. We adopt a pair of frequency selective polarizers (FSP) as a quasi-optical-type SSB filter. A FSP consists of a wire-grid backed by a flat mirror with a small gap. This filter is a modified Martin-Puplett interferometer (MPI) [20] and used for Superconducting Submillimeter-Wave Limb-Emission Sounder (SMILES) [21]. Standing waves are expected to be low in FSP compared with MPI because no rooftop mirror is used. We show the configuration of the FSP for explaining, the principle of the SSB filter and the injection of the LO signal in Fig. 6. They work as a four-port dual beam interferometer with two 45° wire grids. The transmission frequency characteristic of the signal from radio frequency (RF) at Port 1 to a SIS mixer in the receiver at Port 3 is controlled by changing the gap width d between the grid and the flat mirror [21], [22]. The SIS mixer at Port 3 receives signals from Port 1 and Port 2. The width also controls the coupling efficiency from the LO at Port 2 to the SIS mixer at Port 3 (Fig. 6).

We designed the frequency characteristic of the filter to achieve the SSB observation for CO ($J = 4{-}3$) in a lower sideband and [CI] ($^3P_1{-}^3P_0$) in an upper sideband for IF of 7.2 GHz. We found the optimum value of the gap width to be 2.644 mm to transmit two emission lines with high image rejection ratio.

The LO consists of a signal generator unit followed by an amplifier and a multiplier unit. The multiplier unit produces the LO signal whose frequency is 108 times higher than that of original CW signal of 4–5 GHz from the signal generator. The SIS mixer receives thermal noise in the image band from Port 2 in addition to the LO signal. Therefore the thermal emission from LO port increases noise for heterodyne detection in SSB mode. We inserted an additional wire grid in front of the LO port so as to terminate 95% of the thermal emission from the LO port into a cold load in the cryostat.

5) Optical Pointing System: The 30-cm telescope is equipped with an optical pointing system because there is not enough number of bright and point radio sources for the 9′ beam in the 500 GHz band. A monochromatic CCD camera is mounted on the mount of the subreflector. The CCD camera is set with a lens whose the diameter and the focal length are 31.5 mm and 75 mm, respectively. The size of the image is $4.53^\circ \times 3.40^\circ$ and the resolution is 24″/pixel. A R64 filter is attached in front of the lens to cut the scatted light of the sky shorter than wavelength of 640 nm. It enables us to get images of stars that are brighter than 3.5th of magnitude in the twilight. The output of the camera is converted into a digital image by a video capture board for the analysis on a computer.

C. Intensity Calibration

We use the standard chopper-wheel method for the intensity calibration [23], [24]. A switching mirror is inserted between the PM2 and the PM3 in the azimuth axis at certain intervals (Fig. 3). The mirror terminates the beam to a radio absorber (TK-RAM). Temperature of the absorber is monitored so as to obtain the antenna temperature.

D. Receiver System

1) Cryo-Receiver: We adopted a Superconductor-Insulator-Superconductor (SIS) mixer associated with Parallel-Connected Twin Junctions (PCTJ) which was made at the Nobeyama Radio Observatory. The junction consists of niobium and aluminum oxide as the superconductor and the insulator, respectively. It needs no mechanical tuner for impedance matching of the SIS device, and low noise (less than 200 K in DSB mode) is expected. The size of the device is 180 μm × 2.2 mm and its thickness is 90 μm. The area of the junction is about 1 μm^2. The resistance of the device is about 40 Ω at ambient temperature because of the combined resistance of the two junctions is about

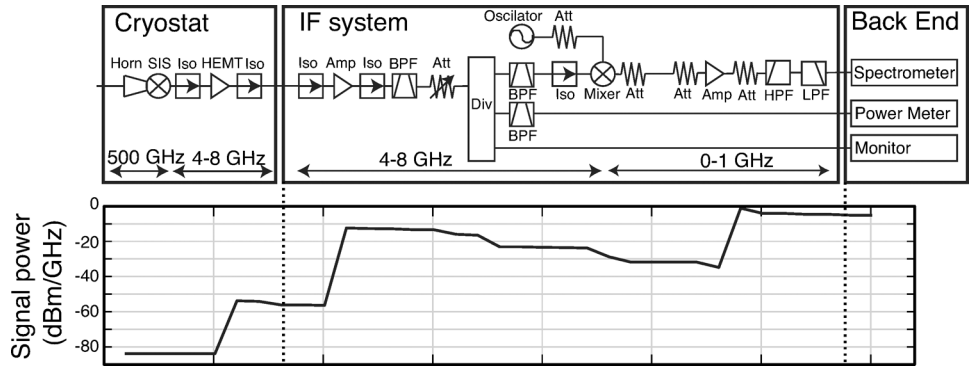

Fig. 7. Block diagram of the receiver system and level diagram of the signal from the feed horn to the spectrometer.

15 Ω and a resistance of microstrip line in the device is about 25 Ω. Two permanent magnets are attached to both sides of the mixer block to give a magnetic field of 140 G to suppress the Josephson current. The device is mounted on a mixer block, which is made of gold plated copper. The RF signal and the LO signal are led to the SIS mixer through the feed horn, which is combined with the mixer block.

We selected a small 4 K Gifford-McMahon cryocooler for cooling down the SIS mixer with the weight and power saving. The cryostat has a cylindrical form and its size is 32 cm in diameter and 50 cm of height. The weight of the cryocooler including the cryostat is about 15 kg and its consumption power is 1.3 kW. These are suitable for the operation at Dome Fuji. The cooling capacities of the 60 K stage and the 4 K stage are 2.5 W and 0.1 W, respectively. A small helium pot is attached to the top of the cryocooler to reduce the fluctuation of temperature of the 4 K stage using its large thermal capacity. A 50 μm-thick film of Kapton is used as a vacuum window of the cryostat. Two Zitex films (G110) are attached on a window of a 60 K shield as infrared scattering filters in the cryostat.

A HEMT amplifier was employed as a first amplifier of the receiver system on the 60 K stage. The consumption power is less than 30 mW. The gain and the noise temperature of the HEMT amplifier are about 30 dB and 6.5 K within the fist IF band, respectively. An isolator is inserted to reduce the reflection of the signal between the HEMT amplifier and the SIS mixer. The isolation level is larger than 30 dB. The SIS mixer is biased through a port of the isolator using a source meter with the four-wire method.

2) IF System: The signal from the cryostat is transmitted to the IF system for adjustment of the level and the frequency to match a back end system. Fig. 7 shows the configuration and a level diagram of the receiver system. The system consists of amplifiers, filters, mixer, attenuators, isolators, a divider and a crystal oscillator. In the system, the first IF signal is amplified by a 40 dB-gain amplifier and filtered by a 4–8 GHz bandpass filter. A step attenuator is inserted to control the level of the signal. Then the signal is divided into three outputs for a continuum observation, a line observation and a monitor. The first output is led to a power sensor for the continuum detection through a 4–8 GHz bandpass filter. The second output is led to a mixer through a 6.7–7.7 GHz bandpass filter. It is down-converted to the second IF signal of 0–1 GHz with a 6.7 GHz signal from the crystal oscillator. The second IF signal is transmitted to a spectrometer after amplified by a 34-dB gain amplifier and filtered by a 40 MHz high-pass filter and a 960 MHz low-pass filter.

E. Back End System

We employ an FX-type 1 GHz spectrometer and a power meter for the back end system. A spectrum is produced as auto correlation of the Fast Fourier Transformation of the 8-bit fast sampled input signal. The 1 GHz wide spectrum consistes of 16384 channels corresponds to frequency channel width of 61 kHz. It covers ±300 km/s in velocity at 500 GHz band that is wide enough to cover observed CO ($J = 4-3$) line width at the Galactic center [7]. The velocity resolution is 0.04 km/s which is much narrower than the typical line width of CO line width of a few km/s for molecular clouds. The linearity of the spectrometer is kept within 5% over 10 dB. An Allan time of more than 300 seconds was measured under stable temperature variation less than 0.5 K. Integration time of the signal is selected as multiples of 1 second. Typically we use 10 seconds integration on source and the observed data is stored on a hard drive of the spectrometer. It is compact with weight of 7 kg and works only at power consumption of 140 W.

F. Control System and Data Acquisition

A central computer controls all instruments of the 30 cm telescope. The computer is connected to a control box of the azimuth and the elevation motors of the antenna, the signal generator of the LO, the biasing power of the SIS device, the power meter, the spectrometer, and a moving mirror for intensity calibration. It also monitors ambient pressure and temperature, and the temperature of the instruments. We developed observation control software based on that used at the Nobeyama Radio Observatory for Doppler tracking and position tracking. The clock of the computer is synchronized to the GPS time. We store spectra and observational logs, such as position of the antenna, in a hard drive of the spectrometer and the central computer, respectively. The observed data and monitoring data are accessible from outside of the telescope through a network system. It is also possible to control the telescope remotely.

IV. Performances

A. Receiver Test at Laboratory

Fig. 8 shows the beam pattern of the feed horn alone measured in the laboratory. We derived the beam pattern from mea-

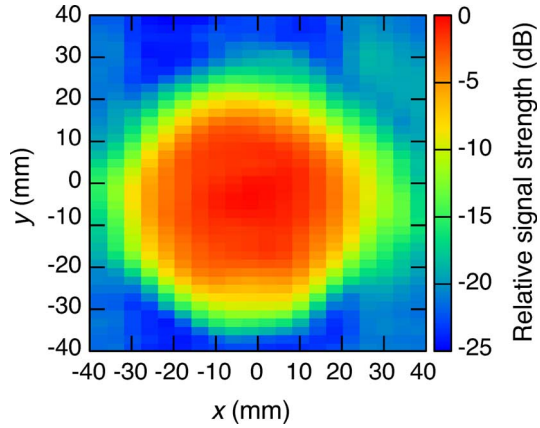

Fig. 8. Beam pattern of the feed horn at 461 GHz. The x-axis and the y-axis represent distance from the origin of the scanning. The color scale represent the relative signal strength normalized to the central peak.

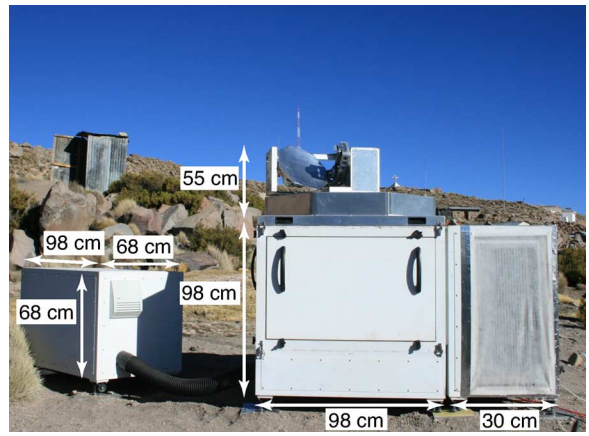

Fig. 9. Photograph of the 30-cm telescope in Chile with its size. The antenna subsystem is placed on 98 cm cube main box.

surement of {the response of the SIS current under a constant biasing voltage by a planar scanning of a 461 GHz source at 142 mm away from the aperture. We checked in advance that the current increased up to 100 μA without significant saturation as we changed the power of the source. The current was controlled below 100 μA during the scanning. We calculated the beam pattern by normalizing the current for each position by the current at the center. The pattern has symmetry shape and its {beam radius} is 26.3 ± 1.3 mm. It is consisted with the designed value of 26.0 mm with correction of the beam pattern of the 461 GHz source. There is no side lobe at a level higher than -25 dB.

The image rejection of the SSB filter was estimated by the measurement of the response of the SIS current also. We measured the current of the SIS by sweeping the frequency of the LO signal. We estimated the gap width to be 2.488 ± 0.006 mm from fitting the frequency characteristic of the FSP. The image rejection ratio was estimated to be -21 ± 4 dB and -17 ± 4 dB for observation of CO $(J = 4 - 3)$ and [CI] $({}^3P_1 - {}^3P_0)$, respectively.

The receiver noise temperature is 900 K in SSB evaluated at the window of the cryostat, that is derived from Y-factor measurement for the output power of the IF system. The rather high noise temperature results from high physical temperature of 4.9 K of the SIS mixer, 60 K of the HEMT, and the loss in the IF cable between the SIS mixer and the HEMT. We are planning to upgrade the cryostat without changing the low power consumption 4 K cryocooler. We will insert an additional IR blocking filter in the window. We will replace the thermal shield made of aluminum with one made of copper. These will significantly reduce the heat input in thermal radiation. Therefore we expect lower temperatures both in the 4 K and 60 K stage. We could also shorten the IF cable.

B. Weight, Size and Power Consumption

All the equipment of the receiver system, the back end system, and the control system, are set in a main box under the antenna system, except the compressor of the cryocooler. The main box is divided into three subsystems to satisfy the weight limit of 60 kg for the transportability. The weight of equipment in the telescope is about 300 kg. The total weight of the whole system of the telescope that includes two generators and five wooden boxes for the transportation is 700 kg. The heaviest of these subsystems is the antenna system whose weight is about 55 kg.

The 30-cm telescope was evaluated by the test observation in Chile during winters of 2010 and 2011 after the laboratory testing. We selected Parinacota in northern Chile as a site for the test observation. It is located about 2000 km north from Santiago and its altitude is 4400 m. The latitude and longitude are $18^\circ 12'$ S and $69^\circ 16'$ W, respectively. We set the 30-cm telescope in Parinacota as shown in Fig. 9. We succeeded in assembling the telescope only by four people within three days.

The electrical power was supplied by two generators. A generator features a sine wave inverter was used stably with computers and various measurement devices that are highly sensitive to changes in frequency and voltage. Its rated voltage and power are AC100 V and 2.8 kW at the sea level. However, the oxygen-poor environment due to high altitude results in a lower power output from the engine. We adjusted the radius of the main jet in the generators to optimize the Air-fuel ratio for high altitude environment. Atmospheric pressure at the site ranges 580–600 hPa, so the power would decrease to about 50% relative to the power at sea level. Therefore we operated generators connected in parallel to have a sufficient power. The total consumption power of the telescope was measured to be 2.4 kW in operation. We attached an external tank to the generator to extend the operation time to longer than 24 hours.

C. Pointing Accuracy

The pointing of the telescope was established by two steps. In the first step the pointing error due to the antenna mount is adjusted by observation of bright stars with the CCD camera on the 30-cm telescope. We selected stars from the Fifth Fundamental Catalog [25] that have magnitude greater than 3.5 with correction of proper motion. The pointing error is removed by optimizing parameters that describe imperfectness of the azimuth and the elevation mounts of the telescope. The position error of stars is recorded as well as the azimuth and elevation offsets. Then these offsets data are fitted with the 15 parameters model with least-squared method. We iterated the pointing three times to converge the model. We represent the distribution

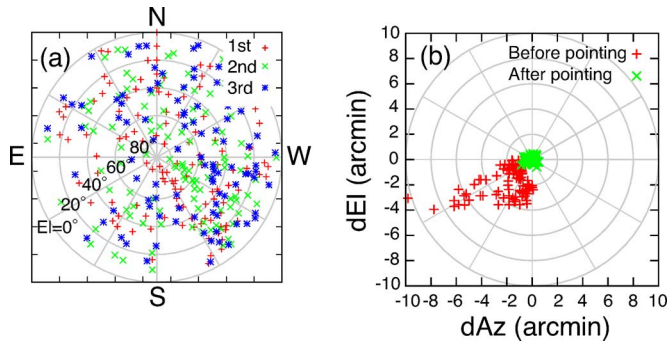

Fig. 10. Result of the optical pointing. (a) The distribution of the observed stars plotted on the celestial sphere. Positions at the 1st, 2nd, and 3rd pointing are represented with red plus, green cross, and blue asterisk, respectively. (b) The residuals of the fit. Red plus as and green cross as represent the error before the 1st pointing and after the 3rd pointing, respectively.

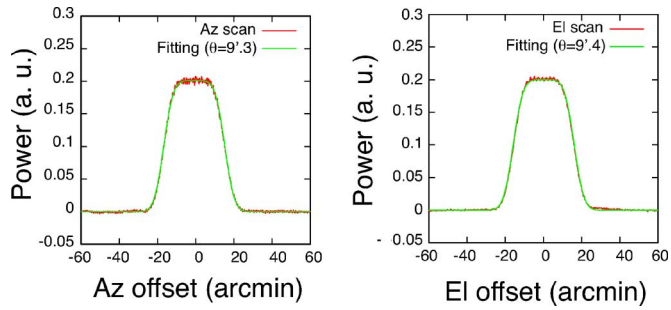

Fig. 11. Results of scanning of the sun (red line) at 461 GHz and the fitting (green line) a model of beam pattern. The left figure is IF output in azimuth direction and the right figure in elevation direction.

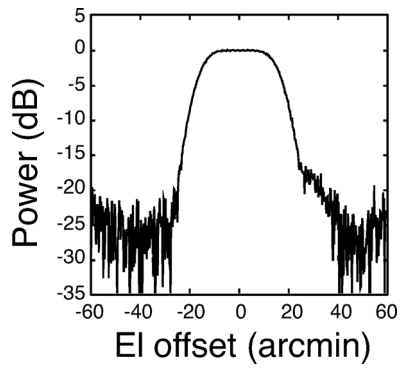

Fig. 12. Result of scanning of the sun at 461 GHz in elevation direction. The data is same as Fig. 11 (right), but the data are plotted in decibels.

of observed stars over the sky in Fig. 10(a). After the fitting, the root mean squared error along azimuth and elevation were $0'.26$ and $0'.22$, respectively. Fig. 10(b) shows that the large residual before pointing (red plus) is corrected to the center of the image at the after pointing (green cross). These errors are less than one-thirty of the angular resolution and are small enough for observations.

In a second step, we aligned the radio axis to the optical axis that was established by the optical pointing. The radio pointing was adjusted by observing bright and compact CO sources such as Orion KL and M17. Final pointing error was $1'$, that is small enough for the $9'$ beam of the 30-cm telescope.

D. Beam Pattern and Angular Resolution

The beam pattern of the antenna was evaluated by scanning the sun. The IF output power (4–8 GHz) was taken by the power meter at 0.1 s intervals while the scanning of the sun at 461 GHz (0.65 mm in wavelength) along in the azimuth and the elevation axes. We inserted a Zitex film in front of the subreflector to attenuate the sunlight in optical and infrared light for protecting the telescope. The IF output is a convolution of the beam pattern $P(x)$ and the brightness distribution of the sun $R(x)$ as follows:

$$f(x) = \int R(x')P(x - x')dx'. \tag{3}$$

The Gaussian beam pattern is evaluated assuming that sun is modeled as a flat uniform circle.

Fig. 11 illustrates the scanning data and the beam pattern in the azimuth (left) and the elevation (right) direction. The red and green lines represent the IF scanning output and the fitting curve, respectively. We fitted the scanning data using the following model, with a, c, d, and θ as free parameters:

$$f(x) = a\left[\mathrm{erf}\left(\frac{(x-c)+b}{\theta/(2\sqrt{\ln 2})}\right) - \mathrm{erf}\left(\frac{(x-c)-b}{\theta/(2\sqrt{\ln 2})}\right)\right] + d \tag{4}$$

where x is scanning angle in the azimuth or the elevation directions, a is a proportionality coefficient depending on intensity of the sun, $b = 16'$ is the apparent radius of the sun, c is the offset between the center of the sun and the scanning origin, d is a constant component depend on radiation from the sky, and θ is angular resolution (HPBW) of the beam of the telescope. The HPBW of the beam in the azimuth and the elevation directions are estimated to be $9'.4 \pm 0'.4$ and $9'.3 \pm 0'.4$ at 461 GHz, respectively. The measured angular resolution is consistent with the designed value of 9'.6. The scanning patterns have symmetrical shape and no significant side lobes. We found a small side lobe at $+22'$ from the center in elevation direction. The level of the side lobe is -16.6 dB to the main beam (Fig. 12).

E. Moon Efficiency and Aperture Efficiency

We derived the moon efficiency η_{moon} using the scanning data as follows:

$$\eta_{\mathrm{moon}} = \frac{\int_{\Omega_{\mathrm{mb}}} P(\theta,\phi)d\Omega}{\int_{\Omega_{\mathrm{moon}}} P(\theta,\phi)d\Omega} = \frac{T_{\mathrm{A}}^*}{T_s} \tag{5}$$

where $P(\theta, \phi)$ is the beam pattern of the telescope, T_A^* is the measured antenna temperature of the new moon, T_s is the brightness temperature of the new moon, which is assumed to be 110 K (brightness temperature at 1 mm, [26]). Ω_{mb} and Ω_{moon} are the solid angle of the main beam and the moon, respectively. We obtained the antenna temperature on the center of the new moon to be 96 ± 6 K from averaging of 4 points toward the center of the moon. The moon efficiency was estimated to be $87 \pm 5\%$ at 461 GHz by (5). The aperture efficiency η_{A} is also calculated to be $70 \pm 4\%$ at 461 GHz from the following equation, assuming that the moon efficiency is regarded as the main beam efficiency:

$$\eta_{\mathrm{A}} = \frac{\eta_{\mathrm{mb}}\lambda^2}{A\Omega_{\mathrm{mb}}} \approx \frac{\eta_{\mathrm{moon}}\lambda^2}{A\Omega_{\mathrm{mb}}} \tag{6}$$

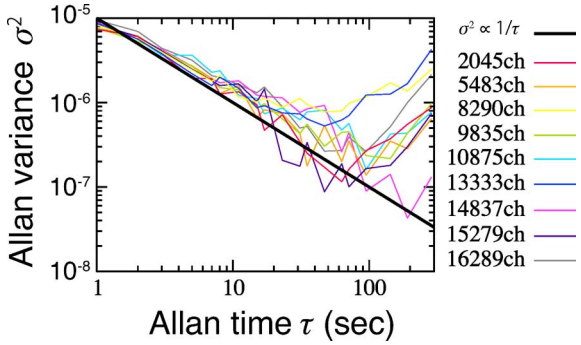

Fig. 13. Results of measurement of the Allan variance at the site. The data at 9 channels are selected randomly from 16384 channels of the spectrometer. The function $\sigma^2(\tau) \propto \tau^{-1}$ is also shown for the comparison with the data.

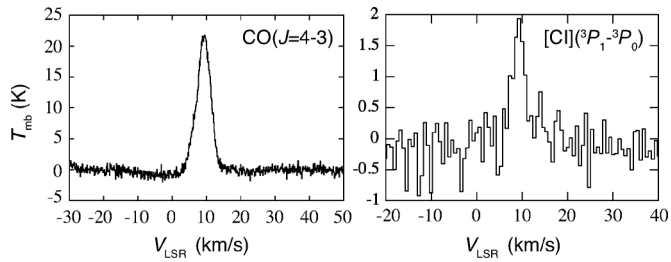

Fig. 14. Spectra of CO ($J = 4 - 3$) and [CI] ($^3P_1 - ^3P_0$) toward Orion KL, the nearest massive star-forming region.

where λ is the wavelength and A is the physical area of the main reflector. This is a reasonable assumption because the angular width of the first null of the beam pattern corresponds roughly to the diameter of the moon. We assumed that $\Omega_{\rm mb} \approx \theta^2$. We also regard the moon efficiency as the main beam efficiency when we derive the main beam temperature of the line.

F. System Noise

The atmospheric opacity at 461 GHz was measured with the tipping-scan method using the telescope at Parinacota. The antenna was programmed to scan the sky from 0° to 80° in the zenith angle. It took about 2 min for one scanning. We selected a direction of scanning to south to avoid the incidence of sunlight. The zenith opacity of the atmosphere ranged 0.6–1.5. The system noise temperature including atmospheric loss was 2000–5000 K during the observation. These values indicate the receiver noise temperature is about 900 K in SSB mode. Therefore there is no discrepancy between the results at laboratory and the observing site. An average of the system noise temperature was 3000 K during observation. We abandoned the observed data with system noise temperature higher than 5000 K.

The ambient temperature changes between -20 °C and 30 °C. A daily minimum temperature increases from -20 °C in early August to -5 °C in late October. It reaches its peak at noon and decreases rapidly after setting of the sun. The relative humidity fluctuate from 20% to 100% at night. On the other hand, it shows steady value of about 10% at the daytime. The atmospheric pressure hovers around 600 hPa, comparable with that at Dome Fuji.

The stability of the receiver system was evaluated by the Allan time at the site. We terminated the receiver with the absorber and recorded the output signal with the spectrometer in a second interval. Fig. 13 shows the Allan variance of several channels as function of the Allan time. The variance of some channels increases from the line of τ^{-1} at about $\tau = 60$ seconds. Although it allows us to integrate for about 30 seconds each on-off interval, the Allan time is shorter than that of the spectrometer alone. We speculate that the results from the gain fluctuation are due to a vibration of the receiver temperature by the cryocooler.

G. First Light Toward Orion KL and Test Observation

We show our first CO ($J = 4 - 3$) and [CI] ($^3P_1 - ^3P_0$) spectra toward Orion KL in Fig. 14. The spectra were obtained in the position-switching mode. The integration time for each scan is 10 seconds. We set the on-position to $\alpha(1950) = 5^{\rm h}32^{\rm m}46^{\rm s} \cdot 5$ and $\delta(1950) = -5°24'14''.0$. The reference position is $+30'$ east of the on-position. We reduced observed data using the "NEWSTAR" package, which is a reduction software developed by the Nobeyama Radio Observatory. The reduction procedure included flagging out bad data, integrating the data in time, and base line subtraction by least-square fitting of a first order polynomial. The intensity of the signal is expressed in main beam temperature corrected by measured main beam efficiency of 87%.

In the CO observation, the total integration time was 760 s. The velocity channel of the spectrum was smoothed to 0.12 km/s of resolution. The peak temperature is 21.7 ± 0.5 K and the integrated intensity from 6 to 12 km/s is 92 ± 2 K·km/s. The peak velocity is 9.4 ± 0.1 km/s and the velocity width (FWHM) of the spectrum is 4.4 ± 0.1 km/s.

In order to assess the adequacy of the data, we compared our CO spectrum with an existing data taken by the 2.2-m ESO telescope at La Silla in Chile [27]. The beam size and the beam efficiency of the 2.2-m telescope are 75″ and 57%, respectively. They estimated that the absolute error of their antenna temperature is less than 20%. The velocity resolution of the spectrometer is 0.3 km/s.

We compared the peak velocity and the integrated intensity of the spectra. The peak velocity ranges between 7.5 km/s and 9.5 km/s within the Orion KL map by the 2.2-m telescope. This agrees with our result because velocity components are mixed within the one beam of the 30-cm telescope. We calculated expected intensity $I_{30\ \rm cm}$ by the following equation so as to compare the integrated intensity taken by different beam sizes:

$$I_{30\ \rm cm} = \frac{\int_{\Omega_{\rm mb}} I_{2.2\ \rm m}(\theta,\phi) P(\theta,\phi) d\Omega}{\int_{\Omega_{\rm mb}} P(\theta,\phi) d\Omega} \tag{7}$$

where $I_{2.5\ \rm m}$ is the integrated intensity taken by the 2.2-m telescope, $P(\theta,\phi)$ is the beam pattern of the 30-cm telescope, which is assumed to be a 2-dimensional Gaussian function with HPBW of $9'.4$. The expected intensity is estimated to be between 86 and 106 K·km/s. This result is also consistent with the observed integrated intensity by the 30-cm telescope, 92 ± 2 K·km/s.

The [CI]($^3P_1 - ^3P_0$) spectrum was taken with 770 s of total integration time. The velocity channels were smoothed to 1.3 km/s to reduce rms of the spectrum in Fig. 14. The peak temperature is 2.0 ± 0.5 K and the integrated intensity is 7 ± 1 K·km/s. The peak velocity is 9.7 ± 1.3 km/s and the velocity width of the spectrum is 5.6 ± 1.3 km/s.

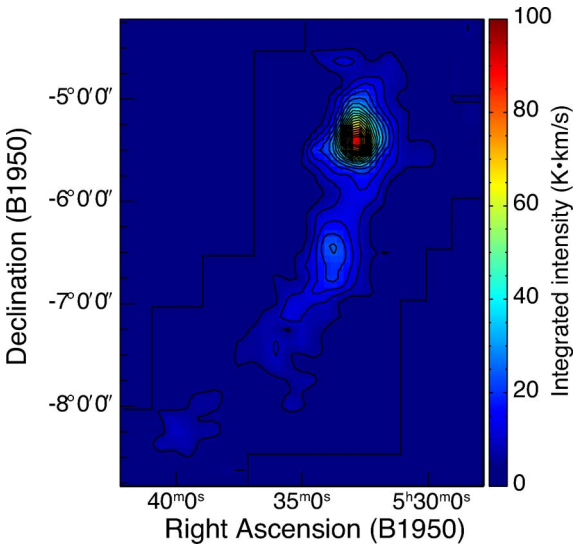

Fig. 15. Integrated intensity map of the CO ($J = 4 - 3$) toward Orion A GMC.

We performed large-scale mapping of CO ($J = 4 - 3$) in Orion A GMC during September and October 2011. Fig. 15 shows the integrated intensity map in the velocity range between 0 and 20 km/s in $v_{\rm LSR}$. We observed a 3 deg-by-4 deg area that includes 690 positions. The achieved rms noise level was 0.5 K after integration of the signal for 5 min per position, which is consistent with the system noise temperature. We also mapped M17 GMC with the CO line.

V. Conclusion

We have developed a transportable 30-cm telescope for a Galactic survey in CO ($J = 4 - 3$) at 461.04 GHz and [CI] ($^3P_1 - ^3P_0$) at 492.16 GHz at the Dome Fuji station in the Antarctic plateau. All systems of the 30-cm telescope were designed to be divided into small subsystems whose mass allowance is restricted to be less than 60 kg for handling only by hand, while keeping the system noise temperature of less than 900 K in the SSB mode. An SIS mixer was employed for the small receiver that has cooling capacity of 0.1 W at the 4 K stage. The 30-cm Offset Cassegrain produced a $9'.4$ beam that was the same beam size as those of Columbia-CfA-U. Chile 1.2 m telescopes for the CO ($J = 1 - 0$) survey and AMANOGAWA telescope for the CO ($J = 2 - 1$) survey.

We operated the 30-cm telescope at a 4400 m-altitude site of Parinacota in northern Chile during winters in 2010 and 2011. We succeeded in assembling the telescope only by four peoples in three days. The typical system noise temperature including the atmosphere was 3000 K (SSB). We made the first observations of CO ($J = 4-3$) and [CI]($^3P_1 - ^3P_0$) lines toward Orion KL using the telescope. We found no discrepancy between our data and existing data in the peak velocity and the integrated intensity. We succeeded in mapping GMCs (Orion A and M17 SW) in the CO line.

We are upgrading the receiver to install a sideband-separating SIS mixer based on ALMA band 8 receiver [28]. We expect to achieve lower noise temperature of the receiver with this upgrading. We will insert thermal insulating sheets (AEROFLEX) on the outer wall of the telescope. We will also cover motors and bearings with heaters and the insulating sheet. Our thermal simulation shows inside temperature of the telescope will be kept above $-20\,^\circ$C under the environmental temperature of $-70\,^\circ$C. The telescope performance will be tested in cold environment in a laboratory. We plan to start the operation of the telescope at Dome Fuji in 2014.

Acknowledgment

The authors would like to thank the Corporación Nacional Forestal (CONAF) in Putre and people in Parinacota for the support during the operation of the telescope in Chile. They acknowledge that the International Foundation High Altitude Research Stations Jungfraujoch and Gornergrat (HFSJG) in Switzerland, made it possible for them to carry out their experiment at the High Altitude Research Station at Jungfraujoch.

References

[1] T. M. Dame, H. Ungerechts, R. Cohen, E. de Geus, I. Grenier, J. May, D. Murphy, L. Nyman, and P. Thaddeus, "A composite CO survey of the entire Milky Way," *Astrophys. J.*, vol. 322, p. 706, 1987.

[2] L. Bronfman, H. Alvarez, R. Cohen, and P. Thaddeus, "A deep CO survey of molecular clouds in the Southern Milky Way," *Astrophys. J. Suppl. Series*, vol. 71, pp. 481–548, 1989.

[3] T. M. Dame, D. Hartmann, and P. Thaddeus, "The milky way in molecular clouds: A new complete co survey," *Astrophys. J.*, vol. 547, no. 2, pp. 792–813, 2001.

[4] P. Solomon, A. Rivolo, J. Barrett, and A. Yahil, "Mass, luminosity, and line width relations of Galactic molecular clouds," *Astrophys. J.*, vol. 319, pp. 730–741, 1987.

[5] S. Sakamoto, T. Hasegawa, M. Hayashi, T. Handa, and T. Oka, "An out-of-plane CO(J = 2 − 1) survey of the Milky Way. I. The data," *Astrophys. J. Suppl. Series*, vol. 100, p. 125, 1995.

[6] T. Yoda, T. Handa, K. Kohno, T. Nakajima, M. Kaiden, Y. Yonekura, H. Ogawa, J. Morino, and K. Dobashi, "The AMANOGAWA-2SB Galactic plane survey I. Data on the galactic equator," *Astronom. Soc. Jpn.*, vol. 62, pp. 1277–1289, 2010.

[7] S. Kim, C. Martin, A. Stark, and A. Lane, "Antarctic submillimeter telescope and remote observatory observations of CO J = 7 − 6 and J = 4 − 3 emission toward the galactic center region," *Astrophys. J.*, vol. 580, p. 896, 2002.

[8] T. Oka, K. Kamegai, M. Hayashida, M. Nagai, M. Ikeda, N. Kuboi, K. Tanaka, L. Bronfman, and S. Yamamoto, "Atomic carbon in the southern Milky Way," *Astrophys. J.*, vol. 623, no. 2, pp. 889–896, 2005.

[9] T. Yamanouchi, N. Hirasawa, M. Hayashi, S. Takahashi, and S. Kaneto, "Meteorological characteristics of Antarctic Inland station, Dome Fuji," *Mem. Nat. Inst. Polar Res.*, pp. 94–104, 2003.

[10] O. Watanabe, K. Kamiyama, H. Motoyama, F. Fujii, H. Shoji, and K. Satow, "The Paleoclimate record in the ice core at Dome Fuji station," *East Antarctica, Ann. Glaciol.*, vol. 29, pp. 176–178, 1999.

[11] S. Ishii, M. Seta, N. Nakai, S. Nagai, N. Miyagawa, A. Yamauchi, H. Motoyama, and M. Taguchi, "Site testing at Dome Fuji for submillimeter and terahertz astronomy: 220 GHz atmospheric-transparency," *Polar Science*, vol. 3, no. 4, pp. 213–221, 2010.

[12] H. Yang *et al.*, "Exceptional terahertz transparency and stability above Dome A, Antarctica," *Astronom. Soc. Pacific*, vol. 122, no. 890, pp. 490–494, 2010.

[13] H. Okita, T. Ichikawa, T. Yoshikawa, R. Lundock, and K. Kurita, "Antarctic infra-red telescope with a 40 cm primary mirror (AIRT40): Development and improvement," in *SPIE Conf. Series*, 2010, vol. 7733, p. 56.

[14] M. Seta, N. Nakai, S. Ishii, M. Nagai, Y. Miyamoto, T. Ichikawa, and N. Takato, "Infrared and THz facilities for Dome F," in *Proc. Int. Astronom. Union*, 2012, vol. 288, pp. 251–255.

[15] K. W. Brown and A. Prata, Jr, "A design procedure for classical offset dual reflector antennas with circular apertures," *IEEE Trans. Antennas Propag.*, vol. 42, no. 8, pp. 1145–1153, 1994.

[16] P. F. Goldsmith, *Quasiopt. Syst.*. : IEEE Press, 1998.

[17] T. S. Chu, "An imaging beam waveguide feed," *IEEE Trans. Antennas Propag.*, vol. 31, no. 4, pp. 614–619, 1983.

[18] K. Pontoppidan, 2002, Technical description of GRASP8. TICRA.

[19] J. F. Johansson and N. D. Whyborn, "The diagonal horn as a submillimeter wave antenna," *IEEE Trans. Microw. Theory Techn.*, vol. 40, no. 5, pp. 795–800, May 1992.
[20] D. Martin, "Polarizing (Martin-Puplett) interferometric spectrometers for the near-and submillimeter spectra," *Infrared Millim. Waves*, vol. 6, pp. 65–148, 1982.
[21] J. Inatani, S. Ochiai, T. Manabe, M. Seta, and R. Wylde, "A new configuration of the Martin-Puplett interferometer with low-reflection," in *IEEE Proc. 7th Int. Conf. on THz Electron.*, 1999, pp. 260–263.
[22] T. Manabe, J. Inatani, A. Murk, R. Wylde, M. Seta, and D. Martin, "A new configuration of polarization-rotating dual-beam interferometer for space use," *IEEE Trans. Microw. Theory Techn.*, vol. 51, no. 6, pp. 1696–1704, Jun. 2003.
[23] B. Ulich and R. Haas, "Absolute calibration of millimeter-wavelength spectral lines," *Astrophys. J. Suppl. Series*, vol. 30, pp. 247–258, 1976.
[24] M. Kutner and B. Ulich, "Recommendations for calibration of millimeter-wavelength spectral line data," *Astrophys. J.*, vol. 250, pp. 341–348, 1981.
[25] W. Fricke *et al.*, "Fifth fundamental catalogue (FK5). Part 1: The basic fundamental stars," *Veroeffentlichung. Astronom. Rechen-Inst. Heidelberg*, vol. 32, pp. 1–106, 1988.
[26] J. Linsky, "A recalibration of the quiet Sun millimeter spectrum based on the Moon as an absolute radiometric standard," *Solar Phys.*, vol. 28, no. 2, pp. 409–418, 1973.
[27] A. Schulz, E. Kruegel, and U. Beckmann, "$CO(J = 4 - 3)$ map of OMC 1," *Astrophys. J.*, vol. 264, pp. 629–636, Oct. 1992.
[28] M. Kamikura *et al.*, "A 385–500 GHz sideband-separating (2SB) SIS mixer based on a waveguide splitblock coupler," *Int. J. Infrared Millim. Waves*, vol. 27, no. 1, pp. 37–53, 2006.

S. Ishii, photograph and biography not available at time of publication.

M. Seta, photograph and biography not available at time of publication.

N. Nakai, photograph and biography not available at time of publication.

Y. Miyamoto, photograph and biography not available at time of publication.

M. Nagai, photograph and biography not available at time of publication.

H. Arai, photograph and biography not available at time of publication.

H. Maezawa, photograph and biography not available at time of publication.

T. Nagasaki, photograph and biography not available at time of publication.

N. Miyagawa, photograph and biography not available at time of publication.

H. Motoyama photograph and biography not available at time of publication.

Y. Sekimoto, photograph and biography not available at time of publication.

L. Bronfman photograph and biography not available at time of publication.